Journal of Power Sources 249 (2014) 59–65

Contents lists available at ScienceDirect

Journal of Power Sources

journal homepage: www.elsevier.com/locate/jpowsour

Reversible phase transformation of titania (anatase) nanotubes upon electrochemical lithium-intercalation observed by *ex situ* transmission electron microscopy

Sovan Kumar Panda [a], Sorae Lee [b], Won-Sub Yoon [b], Hyunjung Shin [b,*]

[a] Fuel Cell and Battery Division, CSIR-Central Glass and Ceramic Research Institute, Kolkata, West Bengal 700032, India
[b] Department of Energy Science, Sungkyunkwan University, Suwon 440746, Republic of Korea

HIGHLIGHTS

- Synthesis of TiO_2 nanotube (NT) array by atomic layer deposition has been reported.
- Li-intercalation in anatase TiO_2 NT curved surface has been investigated by TEM.
- Reversible phase transformation in the NTs was observed in a discharging/charging cycle.
- NTs maintain crystallinity and structural integrity after long cycle run.

GRAPHICAL ABSTRACT

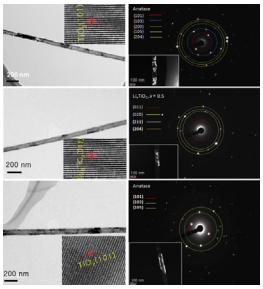

ARTICLE INFO

Article history:
Received 27 June 2013
Received in revised form
4 October 2013
Accepted 14 October 2013
Available online 29 October 2013

Keywords:
Titania nanotube array
Anode material
Lithium-ion battery
Lithium-intercalation

ABSTRACT

In this article, microstructural changes in anatase titania (TiO_2) nanotubes (NTs) upon electrochemical lithium (Li)-insertion/de-insertion using *ex situ* transmission electron microscopy (TEM) have been reported. TiO_2 NT-arrays have been fabricated by coating the wall of the pores of the nanoporous anodic aluminum oxide (AAO) templates using atomic layer deposition (ALD). Anatase TiO_2 NT-array based anode with the wall thickness of ~14 nm shows a reversible discharge capacity of ~175 mAh g^{-1} (i.e., Li-concentration (x) of ~0.53) in the second discharge cycle. The NTs are structurally intact and maintain their high crystalline quality after many repetitions of charging and discharging. Reversible phase transformations from tetragonal (anatase) to orthorhombic (Li-titanate) polymorphs and back to tetragonal (anatase) in complete discharging/charging cycled TiO_2 NTs are observed *ex situ*. Electrical conductivity of the NTs decreases a bit due to lithiation. Arrays of the anatase TiO_2 NTs as anode in Li-ion secondary batteries show satisfactory cycle response and structural stability even after 50 cycles of charging/discharging.

1. Introduction

Design of new electrode materials for Li-ion secondary battery requires the understanding of microstructural changes and/or phase transformations of the material upon electrochemical reactions associated with Li^+ ions. The electrochemical reaction is further reliant on the texture as well as the size of the electrodes' materials. It has been reported that the reduced dimension significantly improves the storage capacity as well as the reaction kinetics *viz.* rate capability by decreasing the ionic and electronic paths, thus diffusion time ($t = L^2/D$, where L is the diffusion length, D is the diffusion constant). Large surface area of the low-

* Corresponding author.
E-mail address: hshin@skku.edu (H. Shin).

0378-7753/$ – see front matter © 2013 Elsevier B.V. All rights reserved.
http://dx.doi.org/10.1016/j.jpowsour.2013.10.048

dimensional structures further provides a wide contact with the electrolyte which can enhance the lithium-ion flux across the interface and thus the power density as a consequence.

Vertically aligned array of the one-dimensional (1D) nanostructures, for example, nanorods, nanowires, nanotubes (NTs) etc., are known as a class of potential electrode material owing to their large exposed surface area compared to the nanoparticle-based electrode with the same diameter or mass. The space between neighboring 1D nanostructures encourages the diffusion of electrolyte into the inner region of the electrode which improves the specific capacity and durability of the cells. The arrayed 1D structure additionally accommodates strain which arises due to the Li-insertion/de-insertion into/from the structure, along a specific orientation without irregular expansion [1–4]. Among the 1D nanostructures, NTs dominate in term of electrode performance on account of their higher surface area (both the inner and outer surfaces can be exposed to the electrolyte) [5–13]. Axial void space of the NTs also accommodates the volume expansion during Li-intercalation and eliminate the internal stress in the material providing excellent cyclability [2,14]. Moreover, vertically oriented NT arrays are quite significant as electrode materials since all the NTs are directly connected to the current collector which facilitates efficient charge transport without using conductive additives and/or binders.

As a safe and potential anode material for Li-ion battery, TiO_2 has been studied extensively since it has very high chemical stability, low self-discharge rate, low fabrication cost and environmentally benign. Anatase is outstanding owing to its reversible uptake of 0.5 Li per formula unit [15] and fast Li-ion insertion and extraction. Anatase structure consists of four octahedrally coordinated Ti atoms and eight three-fold coordinated oxygen atoms. The structure seems a chain of edge-sharing TiO_6 octahedrons where each Ti^{4+} ion is surrounded by six O^{2-} ions. The empty octahedral and tetrahedral sites in the unit cell are coordinated to host Li^+ upon electrochemical insertion. Since the tetrahedral voids are higher energy sites, only octahedral voids are supposed to take part in Li^+ intercalation. The inserted Li^+ in TiO_2 matrix occupy the interstitial octahedral sites in random fashion, where there are four octahedral sites available per primitive cell. The average overall occupation factor of the octahedral sites is restricted by the Li^+-Li^+ repulsive interactions. Tielens et al. [16] reported that up to $x = 0.25$ Li^+ uptake in the anatase structure, there will be only one octahedral void filled out of four in a primitive cell. The filling factor increases with increase in Li concentration which turns out to be two for $x = 0.5$ and four for $x = 1$ (saturated structure where all the octahedral sites are filled). Upon Li^+ insertion, the tetragonal phase TiO_2 (space group: $I4_1/amd$) undergoes a phase transformation to orthorhombic lithium titanate ($Li_{0.5}TiO_2$, space group: *Imma*) through Li-poor TiO_2 solid solution (space group: $I4_1/amd$) [17,18]. The main redox reaction responsible for the electrochemical activity is the conversion of Ti^{4+}/Ti^{3+} during the discharging process and vice versa during the charging process. The overall Li insertion and de-insertion in/from the TiO_2 can be described as:

$$TiO_2 + xLi^+ + xe^- \leftrightarrow Li_xTiO_2 \quad (1)$$

The intercalation properties are reported to be quite different to a large extent from the conventional intercalation kinetics when the size of TiO_2 approaches toward few nanometer and can accept more Li in the structure [19]. It has been reported that particles of 40 nm in diameter can host maximum $x = 0.1$ Li^+ in the structure without forming a new phase and the solubility limit reaches up to $x = 0.22$ for the particle size of 6 nm in diameter [18]. Interestingly, maximum solid solubility limit of Li^+ in the micron-sized/bulk anatase is limited to $x = 0.026$ [20]. Furthermore, the nanoparticles with sizes below 7 nm can host overall lithium concentration $x = 1$ in the structure and completely convert into Li_1TiO_2 with the same space group ($I4_1/amd$) as anatase, but with shifted lattice parameters [21]. With the formation of Li_1TiO_2 ($x = 1$) phase, the structure hosts extra Li compared to the micrometer-sized particles/bulk and the capacity reaches to the theoretical maximum value of ~330 mAh g^{-1} for the anatase TiO_2 [21,22]. Micrometer-sized anatase particles form Li-titanate upon lithiation up to maximum obtainable Li concentration depending on the particle size [22] with the expense of anatase phase. Wagemaker et al. [23] reported the formation of both the anatase and Li-titanate domains in a single micrometer sized particle due to lithiation. Wagemaker et al. [22] and van de Krol et al. [24] further reported that the particle size below 120 nm in diameter shows inexistence of two phase equilibrium in a single particle upon lithiation which turns out to be either anatase or Li-titanate phase. For micrometer sized particles, the Li-titanate phase domains grow by the expense of the anatase phase and the two-phase equilibrium between the anatase TiO_2 and orthorhombic Li-titanate phases is maintained by a continuous Li-ion exchange [25]. The micrometer-sized particles, however, can also be transformed to Li_1TiO_2 phase only at the elevated temperature, but not at room temperature because of the poor ionic conductivity of Li_1TiO_2 phase [26,27]. The poor conductivity arises owing to the complete filling up of the octahedral voids by Li-ions. Rahman et al. [28] compared electrochemical performance of TiO_2 NP and NT-based anodes where NP-based anode showed large irreversible capacity and poor capacity retention after several charging/discharging cycles compared to NT-based anode because of the large exposed surface area and short Li^+ diffusion path length in the NTs. Kim et al. [13] further compared electrochemical performance of anatase TiO_2 NT and NR-based anodes which demonstrates higher reversible capacity and capacity retention after large number of cycle run of the NT-based anodes compared to NRs although rate performance of NR-based anode dominates over NTs because of the higher electrode density.

There have been several reports present on the study of the microstructural change in anatase nanoparticles upon electrochemical Li-intercalation using neutron diffraction, *in situ* XRD, NMR and *in situ* Raman spectroscopy, etc. [24,25,29]. Xiang et al. [30] reported the electrochemically driven amorphous to cubic irreversible phase transformation of the TiO_2 NTs. No further work, however, has been reported so far on the study of intercalation mechanism in polycrystalline TiO_2 tubular structures. Li intercalation mechanism in tubular structure and spherical particles has been shown schematically in Fig. 1. In case of polycrystalline NTs, grains are arranged along the length of the NTs which usually appear nonspherical since thickness of the grains are restricted by the wall thickness of the NTs. Elongated grains in the NTs are narrow in the axial direction which gives rise to two variables like NTs' wall thickness and grain diameter in order to express the system unlike only diameter for the nanoparticles. Moreover, there is no report present on the study of reversible Li-intercalation mechanism in crystalline TiO_2 systems (for instance bulk/nanoparticles/one-dimensional structures) using TEM. Ohzuku et al. [31] reported *ex situ* XRD of Li-titanate phase with various degrees of intercalation which demonstrates that Li-titanate phase can be identified separately from anatase diffraction. In this report, *ex situ* TEM study of reversible phase-transformation in anatase TiO_2 nanotubes, fabricated by template-assisted ALD [32], upon Li^+-intercalation have been presented for the first time. The NTs were found to be stable in ambient and also in TEM even under a long time exposure.

2. Results and discussion

Fig. 2 illustrates the electrochemical performances of anatase TiO_2 NT-array based anodes with the average wall thickness of

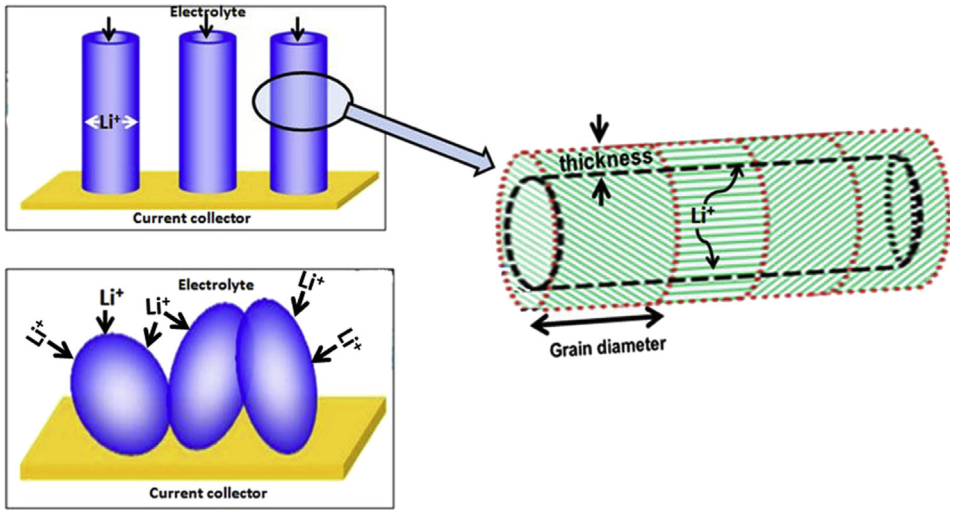

Fig. 1. Schematic diagram of Li-intercalation process in tubular structure and spherical particle-based electrodes.

~14 nm. The first discharge capacity is of ~200 mAh g^{-1} which is corresponding to the Li-concentration of x ~0.60. The reversible capacity is reduced to ~175 mAh g^{-1} (x ~ 0.53) in the second discharging, leaving an irreversible capacities of ~25 mAh g^{-1}. Coulombic efficiency (CE = Charge out/Charge in) in the first cycle is ~87% which increases to 96% in the second cycle and stabilizes at ~ 99% in the 50th cycle. The shape of the charge and discharge curves is in well agreement with our previous report on TiO_2 NT based anode [33] where three zones: sharp decrease in potential region, plateau region and continuous sloped region have prominently been observed. The third discharge capacity is found to decrease slightly (~174 mAh g^{-1}, x ~ 0.52) compared to the second discharge. The capacity decay in this cycle is mainly due to the shortening of the plateau region but the length of the sloped region remains similar to the second discharge. Jiang et al. [19] also reported the shortening of the plateau region with cycling in the nanoparticles based anodes. Appearance of these three main regions in the charge and discharge curves and corresponding Li-intercalation kinetics is well established [2,33–35]. Capacity fading in the first cycle originates from the loss of Li^+ for solid electrolyte interphase (SEI) formation. Stabilization of CE (~99%) indicates negligible capacity fading and very high cyclability of the devices.

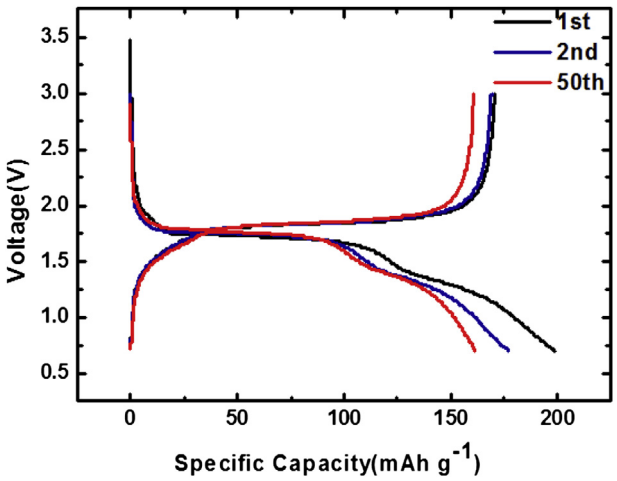

Fig. 2. Electrochemical performance of the anatase TiO_2 NT-based anode in galvanostatic mode using a 0.1 C current rate. Curves of specific capacity vs. voltage were 1st (black), 2nd (blue), and 50th (red) discharging and charging cycles, respectively. (For interpretation of the references to color in this figure legend, the reader is referred to the web version of this article.)

Effect of Li^+-intercalation on the microstructure of anatase–TiO_2 NTs has been studied by high resolution transmission electron microscopy (HR-TEM). Bright field TEM images of Fig. 3a demonstrates that the average outer diameter of the NT is ~80 nm which exactly matches with the average pore diameter of AAOs (Supporting information 1). Average tube wall thickness obtained from the TEM images is ~14 nm, which is corresponding to the coating thickness of 600 ALD cycles (Supporting information 2). Selected area electron diffraction (SAED) pattern (Fig. 3b) reveals that the NTs are crystalline with tetragonal crystal structure corresponding to the anatase phase of TiO_2. Dark field image (inset of Fig. 3b) further indicates that the NTs are polycrystalline. Dark field image of Fig. 3b together with the high resolution images of anatase TiO_2 NTs (Supporting information 3) demonstrate that the NTs consist of large elongated grains. The large grain size facilitates lower resistivity of the individual tubes confirming efficient path way for the electric charges from the redox sites. The NTs do not show any significant change in the morphology (Fig. 3c) after the complete discharge indicating the excellent stability upon Li^+-insertion. SAED pattern of the discharged NTs (Fig. 3d) shows orthorhombic crystal structure indicating a tetragonal to orthorhombic transformation upon Li^+-insertion in the anatase matrix for a Li-concentration of x ~ 0.5. Tielens et al. [16] reported the tetragonal to orthorhombic phase transformation of TiO_2 which begins at the Li-concentration of x = 0.25 at which both the tetragonal and orthorhombic polymorphs have the same formation energy. Above the concentration of x = 0.25, orthorhombic phase formation is energetically favorable and the transition kinetics continues up to the Li-concentration of x = 0.5. The NTs of our interest have average wall thickness of ~14 nm and might be non-uniform in thickness. Some part of the NT wall may go thinner than 7 nm due to non-conformality which may locally host Li^+ up to x = 1 and corresponding capacity should attain ~330 mAh g^{-1}. Volume fraction of such areas, however, is so limited that those not be detected by TEM and their contribution in the electrode performance is not so significant. In general, both the dimensions of the NTs (thickness of ~14 nm and grain diameter of ~250 nm) are large enough compared to ~7 nm which restricts complete transformation to the Li_1TiO_2 phase. On an average, the

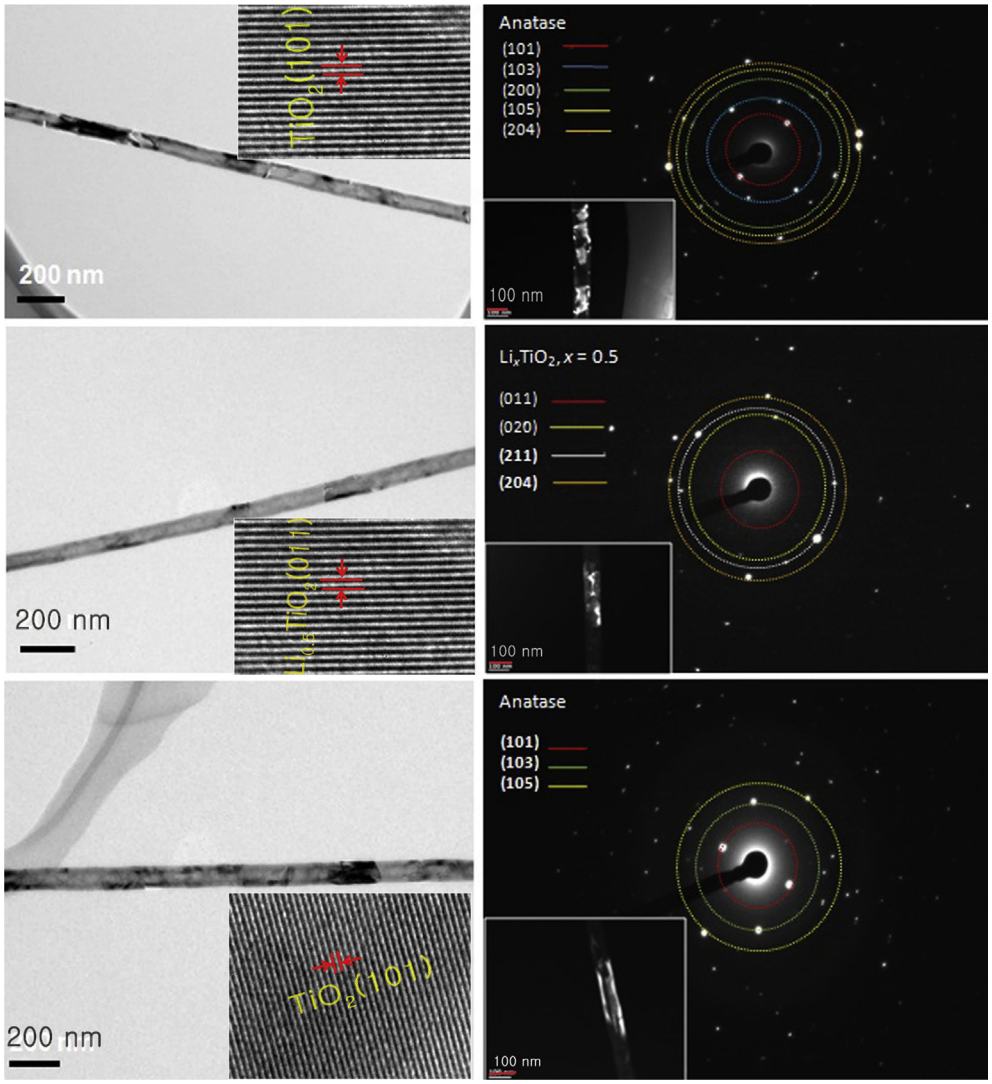

Fig. 3. (a) Bright field TEM image of the anatase TiO_2 NT. Inset shows the high resolution image obtained from an anatase NT with the lattice spacing of 0.35 nm (101). (b) SAED pattern of the NT. Inset shows the dark field TEM image corresponding to (103) spot which shows elongated grains with diameter ~ 250 nm. (c) Bright field TEM image of the discharged NT ($x = 0.5$). Inset show the high resolution image corresponding to the discharged NT with the lattice spacing of 0.35 nm [$Li_{0.5}TiO_2$ (011)]. (d) SAED pattern from the discharged NT matches with orthorhombic phase ($Li_{0.5}TiO_2$). Inset shows the dark field TEM image corresponding to the (211) spot. (e) Bright field TEM image of the charged NT. Inset show the high resolution image corresponding to the charged NT. (f) SAED pattern from the charged NT. Inset shows the dark field TEM image corresponding to the (103) spot.

contribution of $Li_{0.5}TiO_2$ phase is achieved in the electrode performance. Therefore, the reaction mechanism is thought to be analogous to the 14 nm particle system where transformation of the whole anatase grain from the tetragonal to the orthorhombic phase is expected instead of the formation of domain structure by the expense of a large anatase grain. Domain formation further results in an energy penalty due to the phase boundaries. In case the combination of two phases including the phase boundaries has a higher free energy compared to the solid solution, the phase boundaries do not appear and the particle maintain single phase (either solid solution or new phase). In addition, introduction of a phase boundary in 14 nm thick TiO_2 phase leads to an energetically unfavorable situation, and the formation of either anatase or Li-titanate is more favorable which facilitates the complete transformation of the particles [23]. Another dimension, grain diameter (~250 nm) along a tube length, should facilitate the domain structure formation like 250 nm particles [22,23]. Dark field TEM image (inset of Fig. 3d) confirms the large lithium titanate grains with the size similar to the anatase grains (inset of Fig. 3b) which proves that the whole grains have been transformed to the lithium titanate phase. Since Li^+-ion intercalation occurs through the wall of the NTs, the thickness only takes part in the reaction kinetics unlike the grain diameter in the particle system. Fully charged NT (Fig. 3e) also retains similar morphology as the anatase and discharged NTs. The stable structural characteristics render highly reversible Li^+-intercalation and long durability of the cell based on the anatase NTs. SAED pattern of Fig. 3f exhibits a tetragonal anatase structure of the charged NTs which clearly indicates the restoration of the tetragonal structure upon extraction of Li^+ from the orthorhombic Li-titanate structure. Therefore, a reversible tetragonal-orthorhombic-tetragonal phase transformation occurs in a complete discharge–charge cycle. The high-resolution lattice images (inset of Fig. 3a,c and e) further prove that the NTs do not loose crystallinity as well as any further structural integrity upon charging and discharging. In the HRTEM image of Fig. 4, a very thin amorphous sheath layer (thickness ~2 nm) surrounding the NTs has been observed which has also been appeared as diffuse diffraction in the SAED pattern of Fig. 3d and f. The amorphous layer

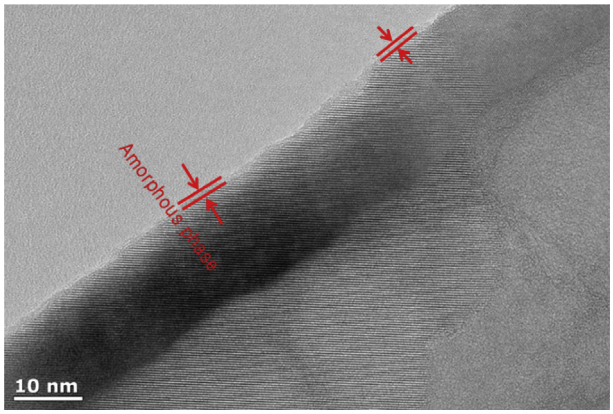

Fig. 4. High resolution TEM image of the lithiated NT which depicts a thin amorphous sheath layer surrounding the NT.

could be the SEI layer and/or Li_2O/LiOH which arises from the oxidation of highly reactive Li_xTiO_2 with oxygen and moisture [36]. This sheath layer may act as a protective layer for the further oxidation of the discharged NTs.

During insertion process, Li^+ undergoes at the empty fourfold-coordinated octahedral void space of the anatase unit cell (Li^+ is positioned in the center of the octahedral void) since the apical oxygen atoms are quite far away. When the Li^+ is displaced a bit in the *c*-direction towards apical oxygen, it becomes fivefold-coordinated. Tielen et al. [16] reported a shifting of Li^+ ion ~ 0.56 Å along *c*-direction for the Li concentration $x = 0.5$. In case of the anatase structure, Li insertion energy decreases with the increase of Li concentration. For a Li concentration of $x = 0.25$, the tetragonal and the orthorhombic forms have the almost equal energies. Therefore, a phase transformation from tetragonal to orthorhombic is most probable from $x = 0.25$ to 0.5. The orthorhombic distortion of the lattice introduces an increase of the Ti–O distances (and the Li–O distances) along *b*-axis whereas the tetragonal anatase and the orthorhombic titanate structures mainly differ in term of the unit cell parameters and not on the octahedron distribution in the space. Beyond $x = 0.5$, according to the phase stability diagram proposed by Wagemaker et al. [22], Li_1TiO_2 start forming and coexists with $Li_{0.5}TiO_2$ for the particle size above 7 nm. For particles below ~7 nm, complete transformation to Li_1TiO_2 upon Li insertion into TiO_2 matrix takes place. In case of larger particles (e.g. ~120 nm), Li_1TiO_2 crystal phase also coexists within one particle with $Li_{0.5}TiO_2$ crystal phase domains but the Li_1TiO_2 domain size would be approximately constant (~4 nm) for different particle sizes [22]. Because of the poor Li^+ ionic diffusivity in Li_1TiO_2 phase, this Li_1TiO_2 phase resides near the surface of the large particles which corresponds to a shell of constant width, surrounding the $Li_{0.5}TiO_2$ core. In this study, average tube thickness is ~14 nm which signifies restriction in the complete formation to Li_1TiO_2 because of the poor Li^+ ionic conductivity in Li_1TiO_2.

For superior cell performance, efficient electron transport between the current collector and the NTs is required. To demonstrate this, current–voltage (*I–V*) measurements of the single TiO_2 NT before and after cycling (complete discharged) have been studied. *I–V* characteristics of Fig. 5a for both the NTs are linear which confirm the Ohmic contact with Ti/Au. The resistance of the anatase TiO_2 NTs (effective length: 10 μm) is ~540 Ω and the corresponding resistivity is $\sim 1.5 \times 10^{-5}$ Ω cm. After Li^+-insertion ($x = 0.53$) in the structure, the resistance of the NTs slightly increases to ~2 kΩ and the resistivity becomes of $\sim 6 \times 10^{-5}$ Ω cm. It is reported that the complete phase transformation from tetragonal to orthorhombic for the Li-concentration of $x = 0.5$ is responsible for the slightly reduction of the conductivity due to the conductivity difference between two phases [36]. The excellent conductivity of both the anatase and lithiated NTs guarantee efficient charge transport during charging/discharging.

Fig. 5b depicts the cycle response of the anatase NT array based anode discharged at 0.1 C current rate up to 50 cycles. The capacity retention at 1st cycle is of ~175 mAh g^{-1} (volumetric capacity ~ 236 mAh cm^{-3}) which diminishes to ~160 mAh g^{-1} (x ~ 0.48) (volumetric capacity ~ 234 mAh cm^{-3}) at 50th cycle. Therefore, ~91% capacity retentions from the first cycle is observed after 50th cycle. Reversible specific capacities based on mass and volume at various discharge cycles have been listed in Table 1. The reversible capacity and the cycle response of the anatase TiO_2 NT based anode are so remarkable which may be due to the unique tubular structures in nanometer scale. Inset of Fig. 5b illustrates the SEM image of the NT array subsequent to 50 cycles run. TEM image of the completely charged and discharged NTs after 50 cycle run has also been illustrated in Supporting information 4. No significant change in the morphology of the NTs was observed even after 50 cycles. With the formation of orthorhombic phase, volume of the unit cell reduces slightly (<2%) compared to the volume of the anatase unit cell [16]. Since the volume contraction due to the formation of $Li_{0.5}TiO_2$ phase is quite small, the stress subjected to the volume change in the discharged NTs is not so significant for which the NTs retain their morphology intact as well as the

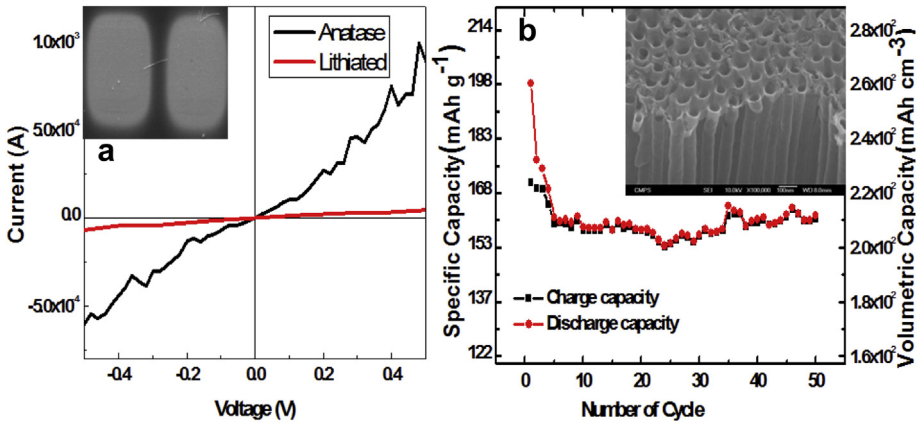

Fig. 5. (a) *I–V* measurements of the single NT before (anatase TiO_2) and after lithiation ($Li_{0.5}TiO_2$). Inset shows FESEM image of the contact in two electrode geometry. (b) Cycle response of the NT array based anode. Inset shows the FESEM image of the NT array after 50 cycle run at 0.1 C.

Table 1
Reversible specific capacities (discharge) based on mass and volume at various cycles.

Number of cycle	Reversible specific capacity (mAh g^{-1})	Li- fraction (x)	Reversible volumetric capacity (mAh cm^{-3})	Coulombic efficiency (%)
1st	175	0.53	236	87
2nd	174	0.52	234	96
50th	160	0.48	210	99

connectivity with the current collector and exhibit superior cycle response.

3. Experimental procedure

3.1. Fabrication of AAO template

Anodic aluminum oxide (AAO) templates were fabricated by well known two-step anodization of high-purity aluminum foils (99.999%, Goodfellow). At first, the aluminum foils (size: 50 × 2 × 0.5 mm^3) were degreased in acetone and rinsed by deionized water and then they were electropolished under a constant voltage of 18 V in a mixture of $HClO_4$ and C_2H_5OH at room temperature for 4 min. The first anodization was performed under a constant voltage of 40 V in 0.3 M oxalic acid (Aldrich) at 10 °C for 5 h. The resulting alumina layer consisted of poor ordering of the pores and hence removed by wet chemical etching in a mixture of phosphoric acid (6 wt.%) and chromic acid (1.8 wt.%) at 60 °C for 1 h. The second anodization was also carried out at identical conditions as the first anodization. The average pore diameter achieved after second anodization was of ~35 nm. Widening of pores was done using 5 wt.% H_3PO_4 at 30 °C for 30 min to have a final pore diameter of ~80 nm. Then, the central aluminum layer was removed in a super-saturated $HgCl_2$ (Aldrich) solution. Finally, AAO membrane of ~20 μm thickness with one open-ended pore was formed.

3.2. Fabrication of titania (TiO_2) NTs

Arrays of TiO_2 NTs were fabricated by coating the wall of pores of AAO template by atomic layer deposition (ALD) using titanium (IV) iso-propoxide (TTIP, UP Chemical) as Ti precursor and water vapor as oxidant. Ar gas with flow rate of 100 sccm was used as carrier and also for purging. Single ALD cycle consisted of an injection of TTIP for 30 s, an Ar purge for 120 s, H_2O vapor pulse for 30 s, and another Ar purge for 120 s. All the depositions were performed at 160 °C with a working pressure of 2.6 Torr. After completion of each cycle, the chamber was evacuated by a rotary pump in order to remove the excess reactants and the reaction by-products. Total time required for the completion of each cycle was 300 s. To fabricate TiO_2 NTs with the wall thicknesses of 14 nm, 600 ALD cycles were performed. As-grown TiO_2 coated alumina membranes were then annealed at 400 °C in air for 1 h in a box furnace.

3.3. Electrochemical measurement

All electrochemical measurements were performed using two-electrode cells. Galvanostatic cycling tests were performed using TiO_2 NTs as working electrodes. As current collector, Ti metal was deposited by e-beam evaporation onto the back side (closed end) of the TiO_2 NTs (Supporting information 5). Prior to Ti deposition, back etching of the TiO_2 coated AAO was carried out by using 1 M aqueous NaOH solution at 30 °C for 1 min to remove the alumina barrier layer from the back side of the NTs to have direct contact between each NT and current collector (Ti film). Li metal was used as the counter electrode. Glass Micro Fibers (Whatman, UK) were used as separators. Electrolyte was a solution of 1 M $LiPF_6$ in 1:1 mixture of ethylene carbonate and dimethyl carbonate. No binders or conducting carbon were used. Cell assembly was carried out in an Ar-filled glove box and packed into a coin cell. The cells were galvanostatically cycled using a Won A Tech WBCS 3000 system and measuring potential was in a potential range of 0.7–3.0 V (Li^+/Li) at current rates from the C/10 (1 C ≡ one lithium per formula unit in 1 h i.e. mA g^{-1}).

3.4. Characterization of titania NTs

Fully charged and discharged cells were broken and electrodes were removed for further analysis and washed thoroughly by dimethyl carbonate and dried in nitrogen flow. The structural and morphological properties of the NTs were characterized by a JEOL-FEM 4010 transmission electron microscope (TEM) operating at 400 kV. For TEM, samples were prepared by dissolving the alumina membrane in 1 M aqueous NaOH solution and dispersing the NTs ultrasonically in de-ionized water and transferring the dispersed solution on a carbon coated copper grid. I–V characteristics of the single NT before and after Li-ion intercalation was measured by dispersing the NTs on SiO_2 (200 nm)/Si wafer and depositing Ti/Au (50 nm/150 nm) films selectively on the NTs with an electrode separations of 10 μm using e-beam evaporator. I–V characteristic was measured using probe station connected with a semiconductor parameter analyzer (Agilent 4155C).

4. Conclusions

TiO_2 nanotubes' arrays based anode show a reversible capacity of ~175 mAh g^{-1} with Li-concentration of x ~0.53. Coulombic efficiency in the first cycle is ~87% which stabilizes at ~99% in the 50th cycle. Discharged NTs are orthorhombic crystal structure and a tetragonal–orthorhombic–tetragonal transformation is clearly observed after a complete discharging–charging cycle. Anatase nanotube array-based anodes show ~91% retention from the first cycle after 50 cycle run. The excellent conductivity of both the anatase and lithiated NTs guarantee efficient electron transport during charging/discharging. NTs do not show any significant morphological change even after 50 charging/discharging cycles which render a long durability of the TiO_2 NT array-based anode.

Acknowledgments

The authors acknowledge financial support from the Agency for Defense Development (ADD), the National Research Foundation of Korea grant funded by the Korean Government (MEST) (NRF-2010-0028972) and by the Human Resources Development program (No. 20124010203270) of KETEP grant funded by the Korean Government Ministry of Knowledge Economy.

Appendix A. Supplementary data

Supplementary data related to this article can be found at http://dx.doi.org/10.1016/j.jpowsour.2013.10.048.

References

[1] C.K. Chan, H. Peng, G. Liu, K. Mc Ilwrath, X.F. Zhang, R.A. Huggins, Y. Cui, Nat. Nanotechnol. 3 (2008) 31–35.
[2] U. Lafont, S. Waichman, M. Valvo, E.M. Kelder, J. Nanosci. Nanotechnol. 10 (2010) 4273–4278.
[3] T. Djenizian, I. Hanju, Y.D. Premchand, F. Vacandio, P. Knauth, Nanotechnology 19 (2008) 205601.

[4] P.L. Taberna, S. Mitra., P. Poizot, P. Simon, J.-M. Tarascon, Nat. Mater. 5 (2006) 567–573.
[5] P. Roy, S. Berger, P. Schmuki, Angew. Chem. Int. Ed. 50 (2011) 2904–2939.
[6] Z. Wei, Z. Liu, R. Jiang, C. Bian, T. Huang, A. Yu, J. Solid State Electrochem. 14 (2010) 1045–1050.
[7] D. Liu, P. Xiao, Y. Zhang, B.B. Garcla, Q. Guo, R. Champion, G. Cao, J. Phys. Chem. C. 112 (2008) 11175–11180.
[8] K. Wang, M. Wei, M.A. Morris, H. Zhou, J.D. Holmes, Adv. Mater. 19 (2007) 3016–3020.
[9] R. Hahn, A. Ghicov, H. Tsuchiya, J.M. Macak, A.G. Munoz, P. Schmuki, Phys. Stat. Sol. A 204 (2007) 1281–1285.
[10] H. Zhang, X.P. Gao, G.P. Li, T.Y. Yan, H.Y. Zhu, Electrochim. Acta 53 (2008) 7061–7068.
[11] Y. Wang, K. Takahashi, H. Shang, G. Cao, J. Phys. Chem. B. 109 (2005) 3085–3988.
[12] M.-H. Park, M.G. Kim, J. Joo, K. Kim, J. Kim, S. Ahn, Y. Cui, J. Cho, Nano Lett. 9 (2009) 3844–3847.
[13] J. Kim, J. Cho, J. Electrochem. Soc. 154 (2007) A542–A546.
[14] T. Song, J. Xia, J.-H. Lee, D.H. Lee, M.-S. Kwon, J.-M. Choi, J. Wu, S.K. Doo, H. Chang, W.I. Park, D.S. Zang, H. Kim, Y. Huang, K.-C. Hwang, J.A. Rogers, U. Paik, Nano Lett. 10 (2010) 1710–1716.
[15] H. Lindstrom, S. Sodergrem, A. Solbrand, H. Rensmo, J. Hjelm, A. Hagfeldt, S.E. Lindquist, J. Phys. Chem. B. 101 (1997) 7717–7722.
[16] F. Tielens, M. Calatayud, A. Beltran, C. Minot, J. Andres, J. Electroanal. Chem. 581 (2005) 216–223.
[17] M.V. Koudriachova, S.W. de Leeuw, N.M. Harrison, Phys. Rev. B. 69 (2004) 054106:1–054106:16.
[18] G. Sudant, E. Baudrin, D. Larcher, J.-M. Tarascon, J. Mater. Chem. 15 (2005) 1263–1269.
[19] C. Jiang, M. Wei, Z. Qi, T. Kudo, I. Honma, H. Zhou, J. Power Sources 166 (2007) 239–243.
[20] M. Wagemaker, G.J. Kearley, A.A. van Well, H. Mutka, F.M. Mulder, J. Am. Chem. Soc. 125 (2005) 840–848.
[21] U. Lafont, D. Carta, G. Mountjoy, A.V. Chadwick, E.M. Kelder, J. Phys. Chem. C. 114 (2010) 1372–1378.
[22] M. Wagemaker, W.J.H. Borghols, F.M. Mulder, J. Am. Chem. Soc. 129 (2007) 4323–4327.
[23] M. Wagemaker, W.J.H. Borghols, E.R.H. van Eck, A.P.M. Kentgens, G.J. Kearley, F.M. Mulder, Chem. Eur. J. 13 (2007) 2023–2028.
[24] R. van de Krol, A. Goossens, E.A. Meulenkamp, J. Electrochem. Soc. 146 (1999) 3150–3154.
[25] M. Wagemaker, A.P.M. Kentgens, F.M. Mulder, Nature 418 (2002) 397–399.
[26] B. Zachachristiansen, K. West, T. Jacobsen, S. Atlung, Solid State Ionics 28 (1988) 1176–1182.
[27] W.J. Macklin, R.J. Neat, Solid State Ionics 53 (1992) 694–700.
[28] M.M. Rahman, J.-Z. Wang, D. Wexler, Y.-Y. Zhang, X.-J. Li, S.-L. Chou, H.-K. Liu, J. Solid State Electrochem. 14 (2010) 571–578.
[29] L.J. Hardwick, M. Holzapfel, P. Novak, L. Dupont, E. Baudrin, Electrochim. Acta 52 (2007) 5357–5367.
[30] H. Xiong, H. Yildirim, Shevchenko, V.B. Prakapenka, B. Koo, M.D. Slater, M. Balasuvramanian, S.K.R.S. Sankaranarayanan, J.P. Greeley, S. Tepavcevic, N.M. Dimitrijevic, P. Podsiadlo, C.S. Johnson, T. Rajh, J. Phys. Chem. C. 116 (2012) 3181–3187.
[31] T. Ohzuku, T. Kodama, T. Hirai, J. Power Sources 14 (1985) 153–166.
[32] H. Shin, D.-K. Jung, J. Lee, M.M. Sung, J. Kim, Adv. Mater. 16 (2004) 1197–1200;
C. Bae, H. Yoo, S. Kim, K. Lee, M.M. Sung, J. Kim, H. Shin, Chem. Mater. 20 (2008) 756–767;
C. Bae, S. Kim, B. Ahn, J. Kim, M.M. Sung, H. Shin, J. Mater. Chem. 18 (2008) 1362–1367.
[33] S.K. Panda, Y. Yoon, H.S. Jung, W.-S. Yoon, H. Shin, J. Power Sources 204 (2012) 162–167.
[34] C.L. Olson, J. Nelson, M.S. Islam, J. Phys. Chem. B. 110 (2006) 9995–10001.
[35] W.J.H. Borghols, D. Lützenkirchen-Hecht, U. Haake, W. Chan, U. Lafont, E.M. Kelder, E.R.H. van Eck, A.P.M. Kentgens, F.M. Mulder, M. Wagemaker, J. Electrochem. Soc. 157 (2010) A582–A588.
[36] R. van de Krol, A. Goossens, E.A. Meulenkamp, J. Appl. Phys. 90 (2001) 2235–2242.